Magnetically induced local lattice anomalies and low-frequency fluctuations in the Mott insulator La$_2$O$_3$Fe$_2$Se$_2$

Riaz Hussain [1], Giacomo Prando [1,*], Sebastian Selter,[2,3] Saicharan Aswartham [2], Bernd Büchner,[2,3,4] and Pietro Carretta[1,†]

[1]*Department of Physics, University of Pavia-CNISM, I-27100 Pavia, Italy*
[2]*Leibniz-Institut für Festkörper- und Werkstoffforschung Dresden, D-01171 Dresden, Germany*
[3]*Institut für Festkörper- und Materialphysik, Technische Universität Dresden, D-01069 Dresden, Germany*
[4]*Würzburg-Dresden Cluster of Excellence ct.qmat, Technische Universität Dresden, D-01062 Dresden, Germany*

We report a study of the Mott insulator La$_2$O$_3$Fe$_2$Se$_2$ by means of ^{139}La nuclear quadrupole resonance (NQR). The NQR spectra evidence a single La site in the paramagnetic phase and two inequivalent La sites, La1 and La2, in the antiferromagnetic phase. These two sites are characterized by different quadrupole couplings, indicative of distinct lattice configurations segregated in domains. The dependence of the quadrupole coupling for La2 on temperature suggests that the structural distortion is driven by the magnetic order parameter. The nuclear transverse relaxation rate $1/T_2$ evidences fluctuations in the paramagnetic phase with characteristic frequencies well below the Heisenberg exchange frequency and likely associated with nematic fluctuations.

The simultaneous occurrence of different microscopic interactions, such as the Coulombic correlations and Hund's coupling, together with the complex fermiology arising from several orbitals crossing the Fermi level make the electronic phase diagram of iron-based pnictides and chalcogenides extremely rich [1–3]. The emergence of orbitally selective Mott transitions, charge disproportionation, and the intrinsic tendency towards phase segregation are exemplary demonstrations of the complexity of these materials [4–7]. Iron-based pnictides and chalcogenides also host an electronic nematic order breaking the C_4 symmetry and leading to a tetragonal-to-orthorhombic lattice distortion [8,9]. Although this phenomenology has been observed in several metallic compounds [10,11], evidence of nematic fluctuations and order in the less studied insulating iron-based materials is still missing.

La$_2$O$_3$Fe$_2$Se$_2$ is an insulator formed by alternating La$_2$O$_2$ and Fe$_2$OSe$_2$ stacked layers and displays antiferromagnetic order below the Néel temperature $T_N \simeq 90$ K [12–14]. The electric crystalline field resolves the Fe orbital degeneracy and drives the system close to an orbital-selective Mott transition, with a suggested relevant role of charge and spin fluctuations [15,16]. Recently, La$_2$O$_3$Fe$_2$Se$_2$ attracted further interest after the report of short-range orthorhombicity both in the paramagnetic phase and in the magnetic phase based on the analysis of the neutron pair distribution function [17]. The breaking of C_4 lattice symmetry has been associated with nematic fluctuations; however, the local orthorhombicity is weakly dependent on temperature, at variance with what is expected for a magnetic driving mechanism.

In order to reach a deeper understanding of the local structure of La$_2$O$_3$Fe$_2$Se$_2$, we used ^{139}La nuclear quadrupole resonance (NQR). NQR is extremely sensitive to the changes in the local charge distribution induced by a modification of symmetry [18,19] and does not require the application of an external magnetic field as in the case of nuclear magnetic resonance (NMR). This is particularly useful when the experiments are performed on powder samples where the broad NMR lines require a more demanding analysis of the results [20]. In this Letter, we report clear evidence of two distinct La sites, La1 and La2, only in the magnetic phase. La1 and La2 are characterized by different quadrupolar couplings, namely, by nonequivalent local structures, suggesting the stabilization of the nematic phase in segregated domains for $T \lesssim T_N$. The temperature dependence of the quadrupole coupling for the La2 site indicates that the structural distortion is driven by the magnetic order parameter. Additionally, measurements of the ^{139}La NQR transverse relaxation rate $1/T_2$ confirm that low-frequency dynamics develop just above T_N, with characteristic frequencies well below the Heisenberg exchange frequency, consistent with the onset of nematic fluctuations in the paramagnetic state which progressively slow down as the temperature is decreased.

We performed the ^{139}La NQR measurements on a La$_2$O$_3$Fe$_2$Se$_2$ polycrystalline sample using a broadband Tecmag Apollo spectrometer [21]. We measured the spectra by recording the amplitude of the echo signal after a Hahn echo pulse sequence ($\frac{\pi}{2}$-τ_e-π) as a function of the irradiation frequency. We derived the spin-lattice relaxation time T_1 by recording the recovery of the nuclear magnetization $M(\tau)$ after a saturation pulse sequence ($\frac{\pi}{2}$-τ-$\frac{\pi}{2}$-τ_e-π) and fitting the data with the functions appropriate for a nuclear spin $I = 7/2$ in NQR [22,23]. We quantified the transverse relaxation time T_2 from the decay of the echo amplitude after a Hahn echo sequence as a function of the interpulse delay, as well as with a
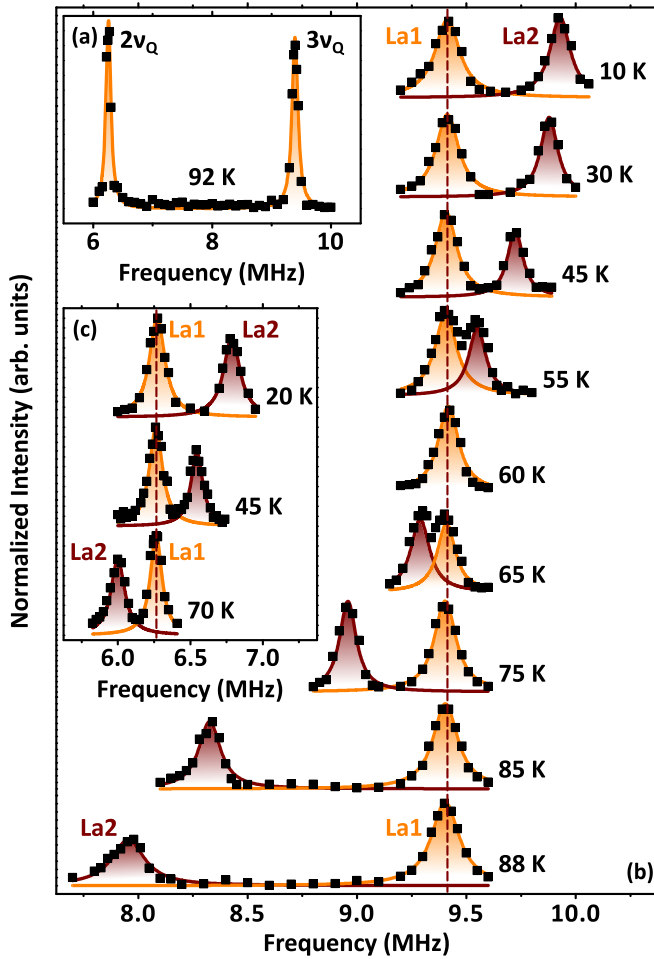
FIG. 1. (a) shows the NQR spectrum at 92 K in the frequency range between $2\nu_Q$ and $3\nu_Q$, proving the disappearance of the La2 signal for $T \geqslant T_N$. NQR spectra at several temperatures below T_N are shown in (b) and (c) ($3\nu_Q$ and $2\nu_Q$, respectively). Orange and dark red lines are best-fitting Lorentzian functions for La1 and La2, respectively.

FIG. 2. (a) shows the temperature dependence of the central resonance frequency of the La1 and La2 signals (solid squares and circles, respectively) at $3\nu_Q$. Open squares and circles represent the central resonance frequency of the La1 and La2 signals, respectively, at $2\nu_Q$ multiplied by a factor of 1.5. (b) reports the signal intensity $M(0)T$ for the La1 and La2 signals at $3\nu_Q$ as a function of temperature. The sharp anomaly at ~60 K is due to the crossing of La1 and La2 signals (see Fig. 1), while the peak at 110 K is an artifact associated with the maximum in the transverse relaxation rate (see Fig. 4).

Carr-Purcell-Meiboom-Gill (CPMG) sequence, which is particularly useful to evidence low-frequency dynamics [24]. In the CPMG pulse sequence, a series of refocusing π pulses are applied at $2\tau_{CPMG}$ intervals after the initial $\frac{\pi}{2}$-τ_{CPMG}-π pulse protocol.

In NQR, the resonance frequency is determined by the interaction of the nuclear electric quadrupole moment eQ with the local electric field gradient (EFG). Given the symmetry of the surrounding charge distribution in $La_2O_3Fe_2Se_2$, in the paramagnetic phase the NQR spectrum is characterized by three lines associated with the $m_I = \pm\frac{1}{2} \leftrightarrow \pm\frac{3}{2}$, $\pm\frac{3}{2} \leftrightarrow \pm\frac{5}{2}$, and $\pm\frac{5}{2} \leftrightarrow \pm\frac{7}{2}$ transitions [21,25]. Here, m_I is the component of the nuclear spin along the EFG main axis Z. These transitions are centered at frequencies ν_Q, $2\nu_Q$, and $3\nu_Q$, respectively, where $\nu_Q = eQV_{ZZ}/14h$, with V_{ZZ} being the main EFG component [21]. Although we performed most of the measurements by irradiating the $3\nu_Q$ line, the measurements at the $2\nu_Q$ transition have proven very useful for the interpretation of our results.

For $T \geqslant T_N$, the $3\nu_Q$ line is centered at ~9.4 MHz [see Fig. 1(a)], in excellent agreement with the estimates of ν_Q

based on NMR [20,21]. The central resonance frequency does not depend on temperature within a few per mil down to 10 K. Hereafter, we shall refer to this NQR signal as La1. The lack of any detectable temperature dependence for the resonance frequency of the La1 signal rules out the development of a sizable internal magnetic field along the Z axis in the antiferromagnetic regime. On the contrary, we cannot exclude the development of a weak internal magnetic field perpendicular to the Z axis based on NQR measurements. Indeed, for $T < T_N$, frequency-swept NMR [21] shows a broadening which is fully consistent with what was reported by Günther *et al.* and described by those authors in terms of a small internal magnetic field perpendicular to the Z axis [20]. A second NQR peak (La2) arises for $T \leqslant T_N$ [see Fig. 1(b)]. Although the temperature dependence of the central resonance frequency of the La2 signal is akin to that of the magnetic order parameter, its frequency shift cannot be associated directly with the internal hyperfine field generated by Fe magnetic moments. In particular, the internal field should lead to a splitting of the ^{139}La NQR peaks [26], and the fact that neither La1 nor La2 peaks split below T_N rather indicates that the internal hyperfine field at ^{139}La is weak (below ~100 G) and/or parallel to the *ab* plane [20,21].

Remarkably, the behavior of the $2\nu_Q$ transition is similar to that observed at $3\nu_Q$ [see Fig. 1(c)]. By scaling the frequency of the La1 and La2 peaks at $2\nu_Q$ by a factor of 1.5 we find a good match with the corresponding $3\nu_Q$ frequencies (see Fig. 2), confirming that the signals are associated with ^{139}La and that the relation $\eta \simeq 0$ holds for the asymmetry parameter for both La1 and La2 [21,27]. These observations also confirm that the frequency shift of the La2 peak is determined by the quadrupolar interaction; that is, its temperature dependence

is determined by the evolution of the local structure around [139]La nuclei.

We estimated the intensity of the NQR spectrum from measurements of $M(0)$, i.e., the initial intensity of the Hahn echo decay, in order to compensate the temperature dependence of the transverse relaxation rate T_2 [21]. The temperature dependence of $M(0)$ is shown in the inset in Fig. 2 after multiplication by temperature in order to account for the paramagnetic character of the nuclear magnetization. $M(0)T$ is approximately constant above T_N, it gets sharply halved at T_N and eventually, below T_N, the intensities of La1 and La2 signals are comparable. We stress that other nuclei, including [77]Se, should have an intensity of the zero-field NMR lines more than an order of magnitude smaller [28].

Overall, our results indicate that one of the La sites remains basically unaffected throughout the whole explored temperature range (La1) while the other site (La2) probes a structural distortion which, remarkably, is segregated in domains with volume weight comparable to the undistorted phase probed by La1. This could explain why the neutron pair distribution function indicates a significant short-range orthorhombicity and an overall long-range tetragonal structure [17]. The dependence of the central resonance frequency for the La2 signal is akin to that of the magnetic order parameter, suggesting that the distortion is driven by magnetism.

The presence of two distinct La sites was already pointed out in the NMR studies by Günther *et al.*, who concluded that two magnetically inequivalent La sites were present with different local hyperfine fields [20]. In fact, our results show that the difference is in the local structure around the La1 and La2 sites. Mössbauer measurements also evidence a small change in the EFG at the Fe site developing below 130 K [17,20]; hence, it is possible that a change in the local structure is already taking place on the Fe_2OSe_2 planes well above T_N and that Fe nuclei in Mössbauer experiments probe an average of the local configurations probed by La1 and La2 sites.

We now turn to the discussion of the low-frequency dynamics. In the paramagnetic phase, we found that the recovery of the [139]La nuclear magnetization by irradiating at $2\nu_Q$ is two times faster than the recovery by irradiating at $3\nu_Q$, consistent with a relaxation mechanism driven by spin fluctuations and not by EFG fluctuations [23]. In the case of relaxation driven by electric quadrupole interactions, the recovery at the two frequencies should be comparable [29]. We show the temperature dependence of the spin-lattice relaxation rate for the La1 and La2 sites at $3\nu_Q$ in Fig. 3. Here, $1/T_1 \propto \omega_e^{-1}$ is approximately constant for $T \gg T_N$, as expected for an insulating paramagnet characterized by the Heisenberg exchange angular frequency ω_e [30]. Upon decreasing temperature, it first shows a weak decrease below about 150 K and then a sharp increase very close to T_N. Below T_N, $1/T_1$ for the La2 site is enhanced with respect to that of the La1 site just below T_N, suggesting a possible contribution from nematic fluctuations. Upon further cooling, $1/T_1$ shows a significant decrease by orders of magnitude with a low-temperature $1/T_1 \propto T^{3.4}$ power law, close to the T^3 law typical of three-dimensional antiferromagnets for $T_N \gg T \gg \Delta$, where Δ is the spin-wave gap [31]. For $T \ll T_N$, the magnitude and behavior of the spin-lattice relaxation rate are qualitatively similar for both La1 and La2 sites. This demonstrates that both the La1 and
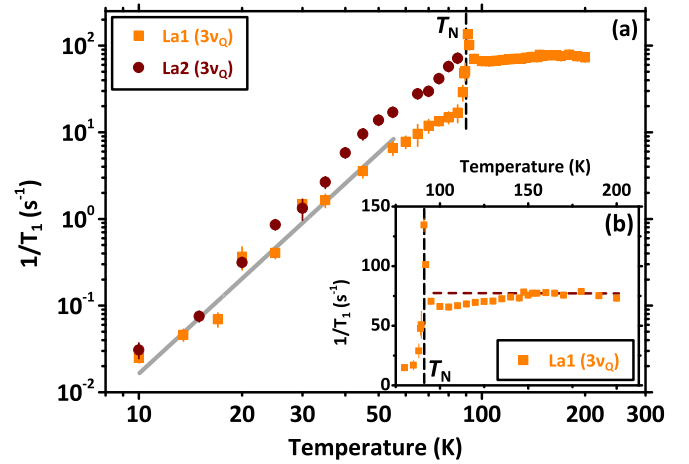
FIG. 3. (a) shows the spin-lattice relaxation rate for La1 and La2 (solid squares and circles, respectively) at $3\nu_Q$ as a function of temperature (log-log scale). The gray line highlights the $1/T_1 \propto T^{3.4}$ power law behavior discussed in the text. (b) highlights the temperature dependence of $1/T_1$ for the La1 signal in the paramagnetic regime (linear-linear scale). The dashed horizontal line is a guide to the eye. In both panels, the dashed vertical line locates T_N.

La2 sites probe the same electronic environment associated with the antiferromagnetic phase of $La_2O_3Fe_2Se_2$. At the same time, the consistent quantitative discrepancies just below T_N support the scenario of segregated domains for La1 and La2 nuclei.

The observed behavior for La1 is analogous to the one derived from NMR measurements [17,20]; however, we outline important differences. In NMR a very slight increase in $1/T_1$ was reported upon decreasing temperature from 150 K to T_N, while here, we observe a decrease in $1/T_1$ [32]. A possible explanation is that in the NMR experiments, given the chosen irradiation frequency, they were probing local field fluctuations in a plane tilted by $\sim 36°$ from the c axis [25]. However, NQR probes fluctuations perpendicular to the Z axis, which is parallel to the crystallographic c axis—in other words, we currently probe fluctuations in the ab plane. Hence, the observed behavior could indicate a progressive decrease of in-plane fluctuations as the temperature decreases. At the same time, for a relaxation mechanism driven by spin fluctuations

$$\frac{1}{T_1} = \frac{\gamma^2}{2} \sum_{\mathbf{q}, \alpha=x,y,z} |A_{\mathbf{q}}|^2 S_{\alpha\alpha}(\mathbf{q}, \omega_R), \qquad (1)$$

where γ is the nuclear gyromagnetic ratio, $S_{\alpha\alpha}(\mathbf{q}, \omega_R)$ are the components of the dynamical structure factor at the resonance frequency ω_R yielding a fluctuating hyperfine field in the ab plane, and $|A_{\mathbf{q}}|^2$ is the form factor describing the hyperfine coupling between [139]La nuclei and the spin excitations at wave vector $\mathbf{q}$. Since for La1 the form factor filters out antiferromagnetic fluctuations, an initial decrease in $1/T_1$ is expected as the spin correlation length starts to increase, similar to what is found in other two-dimensional antiferromagnets [33,34].

Although the temperature dependence of $1/T_1$ at high temperatures is mainly driven by the correlated spin dynamics at frequencies of the order of Heisenberg exchange frequency [30], we find that the temperature dependence of the
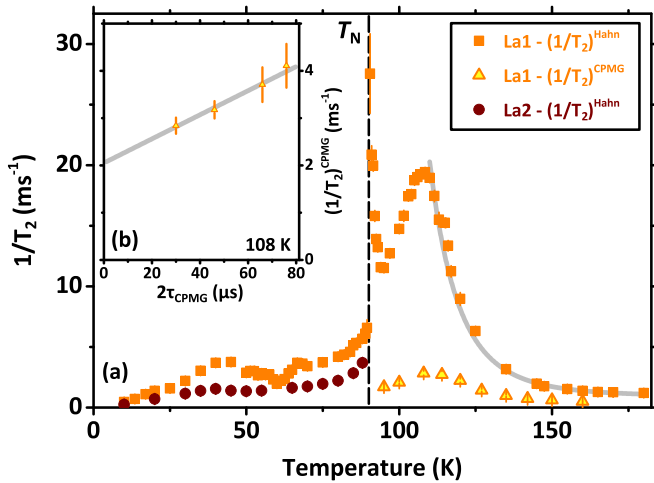
FIG. 4. (a) shows $(1/T_2)^{Hahn}$ for La1 and La2 (solid squares and circles, respectively) at $3\nu_Q$ as a function of temperature. The gray line is a best fit according to an activated Arrhenius law. The open triangles show the temperature dependence of $(1/T_2)^{CPMG}$ at fixed pulse separation ($\tau_{CPMG} = 12$ μs). (b) shows the effect of increasing the pulse separation on $(1/T_2)^{CPMG}$. The gray line is a linear best fit to the data.

transverse relaxation rate $1/T_2$ is determined by low-frequency dynamics (megahertz range). The temperature dependence of $(1/T_2)^{Hahn}$ measured with a Hahn echo sequence at the $3\nu_Q$ transition is shown in Fig. 4; $(1/T_2)^{Hahn}$ shows a well-defined maximum at 108 K, well above T_N. Above the peak temperature, in the limit of fast fluctuations, $1/T_2 \simeq \gamma^2 \langle \Delta h_Z^2 \rangle \tau_c$, with $\langle \Delta h_Z^2 \rangle$ being the mean square amplitude of the field fluctuations along the $Z \parallel c$ axis [35]. Accordingly, we fit the temperature dependence of $(1/T_2)^{Hahn}$ for $T > 110$ K with Arrhenius's law, showing that $\tau_c \propto \exp(E_A/T)$, with $E_A = 1300 \pm 60$ K [see Fig. 4(a)]. In principle, the dynamics leading to this behavior for $(1/T_2)^{Hahn}$ should be probed by $1/T_1$ as well, resulting in a Bloembergen-Purcell-Pound (BPP) behavior [24]. However, the quantitative results found for $(1/T_2)^{Hahn}$ show that this dynamical contribution would lead to $1/T_1 \sim 4$ s^{-1} at the BPP peak. Considering that the spin-lattice relaxation rate is already $\sim$80 s^{-1} for $T > T_N$, it is clear why $1/T_1$ is substantially blind to the low-frequency dynamics probed by $(1/T_2)^{Hahn}$. On the other hand, the divergence of $(1/T_2)^{Hahn}$ at T_N is associated with the critical slowing down of spin fluctuations.

To confirm that the peak in $1/T_2$ at 108 K originates from a progressive slowing down of the fluctuations to very low frequencies, we carried out a study of the echo decay using the CPMG pulsed sequence. The CPMG sequence makes it possible to probe the time evolution of the fluctuations at the La1 site over a shorter timescale τ_{CPMG}. If $\tau_{CPMG} \ll \tau_c$, where τ_c is the characteristic correlation time describing the dynamics, the fluctuations do not have enough time to affect the echo decay, and $(1/T_2)^{CPMG}$ decreases. This is indeed the

behavior we observe which reveals that the fluctuations slow down with τ_c of the order of tens of microseconds around 110 K [see Fig. 4(b)]. Such low frequencies are expected to characterize the dynamics of domains with different degrees of orthorhombicity [36].

The behavior of $1/T_2$ is very similar to that observed in the normal phase of Ba(Fe$_{1-x}$Rh$_x$)$_2$As$_2$ [37,38] and in Li$_2$VOSiO$_4$ [39], a prototype of the J_1-J_2 model on a square lattice. In both cases, dynamics at frequencies orders of magnitude lower than the Heisenberg exchange frequency contribute to $1/T_2$. In particular, a clear difference was reported in $1/T_2$ measured with a Hahn echo and with a CPMG sequence in Rh-doped BaFe$_2$As$_2$ [37]. Moreover, the low-frequency dynamics are characterized by an activated correlation time $\tau_c \propto \exp(E_A/T)$ both in Ba(Fe$_{1-x}$Rh$_x$)$_2$As$_2$ and in Li$_2$VOSiO$_4$, with E_A of the order of hundreds of kelvins for Ba(Fe$_{1-x}$Rh$_x$)$_2$As$_2$ in the presence of a magnetically ordered ground state. In a simple J_1-J_2 model the energy barrier characterizing the nematic fluctuations is the one separating degenerate collinear spin ground states, with E_A depending on J_1 and J_2 and on the spin correlation length. However, the appropriate model to describe La$_2$O$_3$Fe$_2$Se$_2$ is not a pure J_1-J_2 model on a square lattice since there are two different next-nearest-neighbor superexchange paths: one through Se (J_2) and one through O ions (J_2') [40]. This leads to a more complex scenario in which more degenerate phases could be present and requires an accurate theoretical modeling of the system.

In conclusion, we used ^{139}La NQR to study the local lattice modifications induced by the onset of the magnetic order in La$_2$O$_3$Fe$_2$Se$_2$ and the low-frequency dynamics developing in the paramagnetic phase. The presence of two distinct NQR peaks for $T < T_N$ indicates two different structural configurations arising in the magnetic phase. The dependence of the quadrupole coupling on temperature shows that the structural distortion is induced by the development of the magnetic order parameter. The study of the spin-lattice and transverse relaxation rates shows that very low frequency dynamics, at frequencies in the megahertz range, emerge in the normal phase, consistent with the development of nematic fluctuations. Future studies are needed to clarify the local differences between the two La sites.

[1] I. I. Mazin, D. J. Singh, M. D. Johannes, and M. H. Du, Unconventional Superconductivity with a Sign Reversal in the Order Parameter of LaFeAsO$_{1-x}$F$_x$, Phys. Rev. Lett. **101**, 057003 (2008).

[2] K. Kuroki, S. Onari, R. Arita, H. Usui, Y. Tanaka, H. Kontani, and H. Aoki, Unconventional Pairing Originating from the Disconnected Fermi Surfaces of Superconducting LaFeAsO$_{1-x}$F$_x$, Phys. Rev. Lett. **101**, 087004 (2008).

[3] Q. Si, R. Yu, and E. Abrahams, High-temperature superconductivity in iron pnictides and chalcogenides, Nat. Rev. Mater. **1**, 16017 (2016).

[4] L. de' Medici, G. Giovannetti, and M. Capone, Selective Mott Physics as a Key to Iron Superconductors, Phys. Rev. Lett. **112**, 177001 (2014).

[5] L. de' Medici, Hund's Induced Fermi-Liquid Instabilities and Enhanced Quasiparticle Interactions, Phys. Rev. Lett. **118**, 167003 (2017).

[6] A. Isidori, M. Berović, L. Fanfarillo, L. de' Medici, M. Fabrizio, and M. Capone, Charge Disproportionation, Mixed Valence, and Janus Effect in Multiorbital Systems: A Tale of Two Insulators, Phys. Rev. Lett. **122**, 186401 (2019).

[7] M. Chatzieleftheriou, M. Berović, P. Villar Arribi, M. Capone, and L. de' Medici, Enhancement of charge instabilities in Hund's metals by breaking of rotational symmetry, Phys. Rev. B **102**, 205127 (2020).

[8] R. M. Fernandes, A. V. Chubukov, and J. Schmalian, What drives nematic order in iron-based superconductors, Nat. Phys. **10**, 97 (2014).

[9] S. Nandi, M. G. Kim, A. Kreyssig, R. M. Fernandes, D. K. Pratt, A. Thaler, N. Ni, S. L. Bud'ko, P. C. Canfield, J. Schmalian, R. J. McQueeney, and A. I. Goldman, Anomalous Suppression of the Orthorhombic Lattice Distortion in Superconducting Ba(Fe$_{1-x}$Co$_x$)$_2$As$_2$ Single Crystals, Phys. Rev. Lett. **104**, 057006 (2010).

[10] A. E. Böhmer, T. Arai, F. Hardy, T. Hattori, T. Iye, T. Wolf, H. v. Löhneysen, K. Ishida, and C. Meingast, Origin of the Tetragonal-to-Orthorhombic Phase Transition in FeSe: A Combined Thermodynamic and NMR Study of Nematicity, Phys. Rev. Lett. **114**, 027001 (2015).

[11] E. Gati, A. E. Böhmer, S. L. Bud'ko, and P. C. Canfield, Bulk Superconductivity and Role of Fluctuations in the Iron-based Superconductor FeSe at High Pressures, Phys. Rev. Lett. **123**, 167002 (2019).

[12] J. M. Mayer, L. F. Schneemeyer, T. Siegrist, J. V. Waszczak, and B. Van Dover, New layered iron-lanthanum-oxide-sulfide and -selenide phases: Fe$_2$La$_2$O$_3$E$_2$ (E = S, Se), Angew. Chem., Int. Ed. **31**, 1645 (1992).

[13] J.-X. Zhu, R. Yu, H. Wang, L. L. Zhao, M. D. Jones, J. Dai, E. Abrahams, E. Morosan, M. Fang, and Q. Si, Band Narrowing and Mott Localization in Iron Oxychalcogenides La$_2$O$_2$Fe$_2$O(Se, S)$_2$, Phys. Rev. Lett. **104**, 216405 (2010).

[14] D. G. Free and J. S. O. Evans, Low-temperature nuclear and magnetic structures of La$_2$O$_2$Fe$_2$OSe$_2$ from x-ray and neutron diffraction measurements, Phys. Rev. B **81**, 214433 (2010).

[15] G. Giovannetti, L. de' Medici, M. Aichhorn, and M. Capone, La$_2$O$_3$Fe$_2$Se$_2$: A Mott insulator on the brink of orbital-selective metallization, Phys. Rev. B **91**, 085124 (2015).

[16] G. Jin, Y. Wang, X. Dai, X. Ren, and L. He, Strong charge and spin fluctuations in La$_2$O$_3$Fe$_2$Se$_2$, Phys. Rev. B **94**, 075150 (2016).

[17] B. Freelon *et al.*, Nematic fluctuations in iron-oxychalcogenide Mott insulators, npj Quantum Mater. **6**, 4 (2021).

[18] M. Fu, D. A. Torchetti, T. Imai, F. L. Ning, J.-Q. Yan, and A. S. Sefat, NMR Search for the Spin Nematic State in a LaFeAsO Single Crystal, Phys. Rev. Lett. **109**, 247001 (2012).

[19] P. Carretta and G. Prando, Iron-based superconductors: Tales from the nuclei, Riv. Nuovo Cimento **43**, 1 (2020).

[20] M. Günther, S. Kamusella, R. Sarkar, T. Goltz, H. Luetkens, G. Pascua, S.-H. Do, K.-Y. Choi, H. D. Zhou, C. G. F. Blum, S. Wurmehl, B. Büchner, and H.-H. Klauss, Magnetic order and spin dynamics in La$_2$O$_2$Fe$_2$OSe$_2$ probed by ^{57}Fe Mössbauer, ^{139}La NMR, and muon-spin relaxation spectroscopy, Phys. Rev. B **90**, 184408 (2014).

[21] See Supplemental Material at http://link.aps.org/supplemental/10.1103/PhysRevB.103.L081105 for detailed information on the sample synthesis and characterization as well as on the ^{139}La NQR spectra and relaxation measurements. The Supplemental Material includes Refs. [41,42].

[22] D. E. MacLaughlin, J. D. Williamson, and J. Butterworth, Nuclear spin-lattice relaxation in pure and impure indium. I. Normal state, Phys. Rev. B **4**, 60 (1971).

[23] F. Borsa, M. Corti, T. Rega, and A. Rigamonti, Magnetic correlations and ^{139}La NQR relaxation in La$_{2-x}$Sr$_x$CuO$_{4-y}$, Nuovo Cimento Soc. Ital. Fis., D **11**, 1785 (1989).

[24] C. P. Slichter, *Principles of Magnetic Resonance*, 3rd ed. (Springer-Verlag, Berlin, Heidelberg, New York, 1990).

[25] A. Abragam, *Principles of Nuclear Magnetism* (Oxford University Press, Oxford, 1961).

[26] F. Borsa, P. Carretta, J. H. Cho, F. C. Chou, Q. Hu, D. C. Johnston, A. Lascialfari, D. R. Torgeson, R. J. Gooding, N. M. Salem, and K. J. E. Vos, Staggered magnetization in La$_{2-x}$Sr$_x$CuO$_4$ from ^{139}La NQR and μSR: Effects of Sr doping in the range $0 < x < 0.02$, Phys. Rev. B **52**, 7334 (1995).

[27] H. Yasuoka, T. Kubo, Y. Kishimoto, D. Kasinathan, M. Schmidt, B. Yan, Y. Zhang, H. Tou, C. Felser, A. P. Mackenzie, and M. Baenitz, Emergent Weyl Fermion Excitations in TaP Explored by ^{181}Ta Quadrupole Resonance, Phys. Rev. Lett. **118**, 236403 (2017).

[28] According to commercial NMR tables, the absolute sensitivity at constant field, referred to ^{1}H, is 5.91×10^{-2} for ^{139}La and 5.25×10^{-4} for ^{77}Se. Working at constant frequency, the difference is even larger. On the other hand, the fact that one is irradiating just one of the three NQR transitions of ^{139}La causes a reduction in the intensity of $3\nu_Q$ transition by a factor of the order of unity.

[29] A. Campana, R. Cantelli, F. Cordero, M. Corti, and A. Rigamonti, Anelastic relaxation and around the critical Sr content $x = 0.02$, Eur. Phys. J. B **18**, 49 (2000).

[30] T. Moriya, Nuclear magnetic relaxation in antiferromagnetics, Prog. Theor. Phys. **16**, 23 (1956).

[31] D. Beeman and P. Pincus, Nuclear spin-lattice relaxation in magnetic insulators, Phys. Rev. **166**, 359 (1968).

[32] Freelon *et al.* report $1/T_1T$ data for which the $1/T$ factor yields an additional enhancement of the data at lower temperature [17]. We further remark that since La$_2$O$_3$Fe$_2$Se$_2$ is an insulator, there is no reason to report $1/T_1T$ as commonly done in metals for which this quantity is used to evidence the departure from a Fermi liquid behavior.

[33] P. Carretta, T. Ciabattoni, A. Cuccoli, E. Mognaschi, A. Rigamonti, V. Tognetti, and P. Verrucchi, Spin Dynamics and Magnetic Correlation Length in Two-Dimensional Quantum

Heisenberg Antiferromagnets, Phys. Rev. Lett. **84**, 366 (2000).

[34] L. Bossoni, P. Carretta, R. Nath, M. Moscardini, M. Baenitz, and C. Geibel, NMR and μSR study of spin correlations in SrZnVO(PO$_4$)$_2$: An $s = 1/2$ frustrated magnet on a square lattice, Phys. Rev. B **83**, 014412 (2011).

[35] M. Takigawa and G. Saito, Evidence for the slow motion of organic molecules in (TMTSF)$_2$ClO$_4$ extracted from the spin echo decay of ^{77}Se NMR, J. Phys. Soc. Jpn. **55**, 1233 (1986).

[36] A. P. Dioguardi, M. M. Lawson, B. T. Bush, J. Crocker, K. R. Shirer, D. M. Nisson, T. Kissikov, S. Ran, S. L. Bud'ko, P. C. Canfield, S. Yuan, P. L. Kuhns, A. P. Reyes, H.-J. Grafe, and N. J. Curro, NMR evidence for inhomogeneous glassy behavior driven by nematic fluctuations in iron arsenide superconductors, Phys. Rev. B **92**, 165116 (2015).

[37] L. Bossoni, M. Moroni, M. H. Julien, H. Mayaffre, P. C. Canfield, A. Reyes, W. P. Halperin, and P. Carretta, Persistence of slow fluctuations in the overdoped regime of Ba(Fe$_{1-x}$Rh$_x$)$_2$As$_2$ superconductors, Phys. Rev. B **93**, 224517 (2016).

[38] L. Bossoni, P. Carretta, W. P. Halperin, S. Oh, A. Reyes, P. Kuhns, and P. C. Canfield, Evidence of unconventional low-frequency dynamics in the normal phase of Ba(Fe$_{1-x}$Rh$_x$)$_2$As$_2$ iron-based superconductors, Phys. Rev. B **88**, 100503(R) (2013).

[39] P. Carretta, R. Melzi, N. Papinutto, and P. Millet, Very-Low-Frequency Excitations in Frustrated Two-Dimensional $s = 1/2$ Heisenberg Antiferromagnets, Phys. Rev. Lett. **88**, 047601 (2002).

[40] B. Freelon, Z. Yamani, I. Swainson, R. Flacau, B. Karki, Y. H. Liu, L. Craco, M. S. Laad, M. Wang, J. Chen, R. J. Birgeneau, and M. Fang, Magnetic and structural properties of the iron oxychalcogenides La$_2$O$_2$Fe$_2$OM_2 (M = S,Se), Phys. Rev. B **99**, 024109 (2019).

[41] M. H. Cohen and F. Reif, Quadrupole effects in nuclear magnetic resonance studies of solids, Solid State Phys. **5**, 321 (1957).

[42] T. P. Das and E. L. Hahn, Nuclear Quadrupole Resonance Spectroscopy, *Solid State Phys., Suppl. 1*, edited by F. Seitz and D. Turnbull (Academic Press, New York, 1958).